Pergamon

*Applied Geochemistry*, Vol. 9, pp. 701–711, 1994

0883–2927/94 $7.00+0.00

0883–2927(94)E0025–5

# Rare earth element mobility during conversion of nepheline syenite into lateritic bauxite at Passa Quatro, Minais Gerais, Brazil

B. Boulangé and F. Colin

ORSTOM, UM GECO, Laboratoire de Géosciences de l'Environnement, Université Aix Marseille III, 13397 Marseille Cédex 20, France

(*Received* 10 *July* 1992; *accepted in revised form* 4 *May* 1994)

**Abstract**—In a lateritic bauxite formed by weathering of nepheline syenite at Passa Quatro, Minas Gerais State, Brazil, bauxites on the hill-tops directly develop from the syenite bed-rock, while downslope, a kaolinitic layer occurs between bauxite and syenite. A petrological investigation was performed on undisturbed weathered rock samples collected from a representative upslope pit. The undisturbed weathered rocks were chemically analysed for major and trace elements including REE and Zr. Mass balance calculations were applied, and the behaviour of the REE in the Passa Quatro weathering system was established compared to REE reference chondrite and to REE reference parent rock. In the lateritic bauxite, the results suggest that the first stages of weathering induce a volumetric change of 50%, i.e. collapse, with respect to the parent rock, and remove REE with a slightly larger loss of the LREE, except Ce, compared to the HREE. In the upper layers, where bauxite is more mature, a net mass gain in REE is observed relative to the underlying layers. This gain takes place during the reduction of the upper layer during the downward progression of the weathering front. Very significant REE losses occurs during the bauxitization processes throughout the upslope profile. In addition, the downslope kaolinitic system is demonstrated to be depleted in REE in the same proportions as the upslope bauxite. We propose that the REE exported in solution from the whole weathering mantle have enriched neighbouring watershed sediments.

## INTRODUCTION

In a review of rare earth elements (REE) in sedimentary rocks, McLennan (1989) writes: "The nature of REE distribution during mineralogical reactions associated with weathering is very poorly understood". Several field-based studies have suggested that the REE are mobile during weathering but there is little agreement regarding the overall magnitude or the potential for their fractionation. Balashov *et al.* (1964), in a study of sediments from the Russian Platform, were probably the first to have shown that the REE are mobilized during intense chemical weathering under warm and humid conditions and they suggested that the heavy REE are preferentially transported in solution. In contrast, Ronov *et al.* (1967) from studies of weathering profiles on various rock types from Russia, and Duddy (1980) from profiles on Australian volcanogenic sandstone, emphasized that REE were not mobile during weathering. The REE are also believed to accumulate within iron crusts developed from Senegalese sandstone (Steinberg and Courtois, 1976). In many cases, weathering results in the formation of authigenic clay minerals and REE are easily adsorbed at the surface of clay-minerals, such as smectite or kaolinite (Roaldset, 1973; Aagard, 1974; Decarreau *et al.*, 1979; Laufer *et al.*, 1984). Alderton *et al.* (1980) concluded that granite weathering provokes a strong loss of light REE (LREE) (La, Ce, Nd, Sm, Eu) and only a slight loss of heavy REE (HREE) (Gd, Dy, Er, Yb, Lu). The behaviour of REE in bauxitic lateritic profiles has been rarely studied and only karstic bauxite deposits have been examined (Maksimovic and Roaldset, 1976; Maksimovic and Pantó, 1985). These authors have restricted their study to the determination of a Nd-rich synchisite (fluorocarbonate of bastnaesite group) and Nd-rich goyazite (aluminium phosphate of crandallite group) in bœhmite-rich bauxite.

REE analyses are usually normalized to chondritic REE composition. As McLennan (1989) notes that "because of significant volume changes associated with weathering, it is especially difficult to interpret differences in absolute abundances". Such studies could be greatly improved by carrying out mass balance calculations on REE-bearing weathered rock compared to parental fresh rocks. Attempts have been made to account for volume changes (Duddy, 1980) or assumptions made based on the immobility of elements other than REE (Nesbitt, 1979; Middelburg *et al.*, 1988). A good account on the mobility of the REE during weathering of continental rocks is given by Nesbitt (1979) who systematically studied the gains and losses of REE through weathering of a granodiorite in Torrongo, Australia. Assuming Ti is immobile during weathering, Nesbitt (1979) demonstrated that HREE are more enriched than LREE, and he postulated that the REE have been added to the weathering system in association with residual clay minerals, filling the fractures. These have acted as avenues of transport to down-

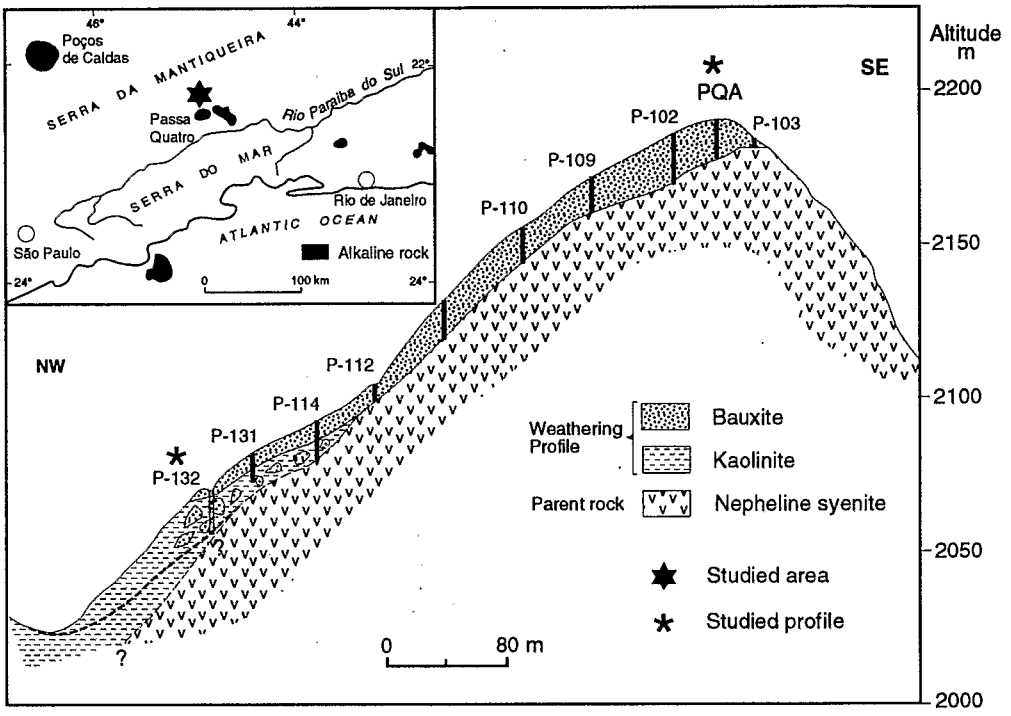


FIG. 1. Geographic setting of the Passa Quatro deposit and cross-section showing the location of pits and the distribution of weathering layers. Particularly the PQA profile and partially P132 were studied for REE distribution. The complete sequence was studied by SIGOLO (1988).

ward translocate the residual material from the upper part of the profile.

Our paper addresses the behaviour of REE within the lateritic bauxite profile developed from weathering of nepheline syenite. Mass balance calculations are applied on weathered rock petrographically studied. A quantitative study of REE behaviour within this weathering environment should contribute to a more complete understanding of REE mobility, and have implications in the interpretation of sedimentary REE patterns, and could be useful in determining landscape palaeoevolution.

## SAMPLING AND EXPERIMENTAL METHODS

The syenitic massif, located at Passa Quatro, Minas Gerais State, Brazil, is one of several alkaline late Cretaceous intrusions (nepheline syenites, microsyenites, tinguaites and phonolites) within the Precambrian basement. The minimum age recorded for the alkaline rocks is 70 Ma (ULBRICH and GOMES, 1981). Several test pits were dug at Alto das Posses (Fig. 1), a locality within the Passa Quatro massif, to study the weathering mantle. Detailed REE analyses were performed on one typical bauxitic profile (PQA) located at the top of the hill. The samples of fresh and weathered rocks were collected after macroscopic description in the field. Undisturbed samples were collected for petrographic study, mineral determinations, chemical microanalyses and density measurements. Sample locations are shown in Fig. 2. The distribution of samples by type of layer within the bauxite profile is from the base to the top: (1) a sample of the fresh nepheline syenite; (2) a sample of the friable saprolite; (3) three samples of the massive

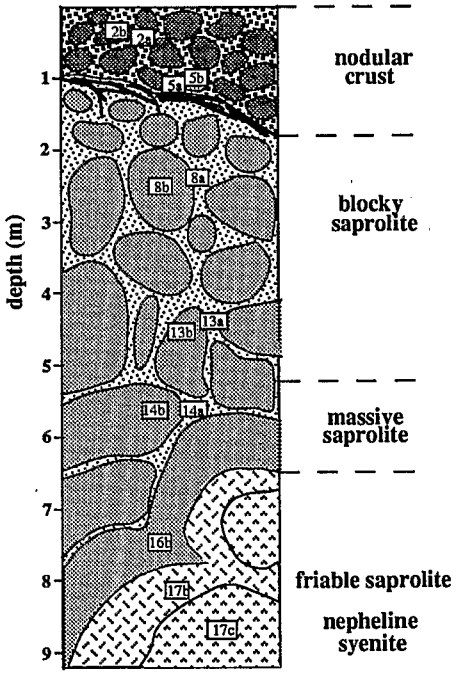


FIG. 2. Sketch of the PQA weathering profile and sample location. The number indicates the sample, the index indicates the matrix—a, the bauxite or bauxitic fragments—b, and the syenite—c.

Table 1. Physical properties of the PQA samples for the matrices (a), the bauxitic fragments (b) and the nepheline syenite (c): bulk density ($\rho_w$), grain density ($\rho_g$), porosity ($\phi$) and volumetric change ($\varepsilon_{Zr}$)

| Sample* | Depth (m) | $\rho_w$ (g/cm$^3$) | $\rho_g$ (g/cm$^3$) | Φ (%) | Zr (ppm) | $\varepsilon_{Zr}$ |
|---|---|---|---|---|---|---|
| 2b | −0.50 | 1.77 | 2.45 | 28 | 2083.26 | −0.52 |
| 2a | −0.60 | 2.10 | 2.58 | 19 | 2816.36 | −0.70 |
| 5b | −1.10 | 1.62 | 2.44 | 34 | 2288.92 | −0.53 |
| 5a | −1.20 | 2.13 | 2.57 | 17 | 2509.10 | −0.67 |
| 8b | −2.50 | 1.64 | 2.53 | 35 | 2463.41 | −0.52 |
| 8a | −2.60 | 2.02 | 2.52 | 21 | 2241.48 | −0.65 |
| 13b | −4.50 | 1.93 | 2.55 | 24 | 2777.92 | −0.57 |
| 13a | −4.60 | 2.05 | 2.58 | 21 | 2102.54 | −0.69 |
| 14b | −5.50 | 1.49 | 2.57 | 42 | 2344.99 | −0.43 |
| 14a | −5.60 | 2.00 | 2.59 | 23 | 2056.55 | −0.53 |
| 16b | −7.50 | 1.43 | 2.52 | 43 | 2539.69 | −0.52 |
| 17b | −8.20 | 1.46 | 2.58 | 43 | 2641.26 | −0.54 |
| 17c | −9.00 | 2.57 | 2.70 | 1 | 684.31 | 0.00 |

*Sample numbers are keyed to numbers in Fig. 2.

saprolite; (4) four samples of the blocky saprolite; and (5) four samples of the nodular crust. Oriented samples were studied by optical microscopy, and scanning electron microscope (SEM) with an energy dispersive capability spectrometer. Back scattered electron imaging was used. Mineralogical composition was determined by X-ray diffraction (XRD) (Sigolo and Boulangé, 1987; Sigolo, 1988).

The REE contents of rock samples were determined using the method of Govindaraju and Mevelle (1987). Crushed rock samples were decomposed by fusion with $LiBO_2$. The fusion products were dissolved in a complexing acid solution which was passed through a cation-exchange column in which only REE are held. The resins were then washed with 2 N $HNO_3$ to remove all elements but the REE. Then the REE were eluted with 7.25 N $HNO_3$ and analysed by ICP (AES). Major elements (Si, Al, Fe, Ti, Ca, Mg, Na, K, Mn) and trace elements (Y, Zr, Nb) of completely dissolved rock samples were also analysed by ICP (AES).

Bulk density measurements were made on rock samples, with an approximate volume of 10 cm$^3$; $\rho_w$ and $\rho_p$ refer, respectively, to bulk densities of weathered and parent rock. Samples were dried, weighed, coated in molten paraffin wax, and then immersed in water to measure their displaced volume. Bulk densities were estimated by mass per unit volume with errors of about 1%. Grain densities ($\rho_g$) were measured by water picnometer with errors of about 1%. Porosity ($\phi$) was calculated from $\rho_W$ and $\rho_g$ (Eqn 1):

$$\phi = 1 - \rho_W/\rho_g. \quad (1)$$

The interpretation of REE mobility in weathering systems is based on the calculation of losses or gains (in relation to parent rock) and on thorough petrological study. Formal mass balance equations as functional forms of constitutive relationships between weathered material chemical composition, bulk density, porosity and volume change in relation to the corresponding chemical and physical properties of fresh parent rocks are used in our work. Volumetric change ($\varepsilon_{i,w}$) is defined by Eqn (2) (Brimhall and Dietrich, 1987):

$$\varepsilon_{i,w} = \frac{\rho_p}{\rho_w}\frac{C_{i,p}}{C_{i,w}} - 1 \quad (2)$$

in which $\rho$ is the bulk density in g/cm$^3$, $C$ is the concentration in g/100g and the subscript "i" pertains to an element considered as immobile during weathering, the subscripts "p" and "w", respectively, pertain to parent rock and to weathered rock.

Loss or gain of a chemically mobile element "j", either by solute chemical migration or physical transfer, is quantified by the open-system mass transport function ($\tau_{j,w}$) defined by Eqn (3):

$$\tau_{j,w} = \frac{\rho_w C_{j,w}}{\rho_p C_{j,p}}(\varepsilon_{i,w} + 1) - 1. \quad (3)$$

In order to calculate both volumetric changes ($\varepsilon_{i,w}$) and net gain or losses ($\tau_{j,w}$) of any element, it is necessary to identify an immobile element relevant with the physical and chemical paths of the studied weathering system.

Heavy minerals were separated by magnetic separator and heavy liquids on both weathered rocks and fresh syenite. The resultant fraction principally consists of euhedral zircons with a size smaller than 50 $\mu$m, minor amounts of partly weathered sphene, and secondary anatase. Zirconium-mapping and microprobe analyses on polished thin sections of fresh and weathered rocks show that all of the Zr is mineralogically linked to zircons. Euhedral zircons are clearly unweathered and so the chemical immobility of zirconium is demonstrated. However, Colin *et al.* (1992) have demonstrated that within the upper part of the Archean gneiss-derived Dondo Mobi (Gabon) weathering profiles, i.e. bio-pedoturbated non-isostructural related to the parent rock, the translocation of Proterozoic schist-derived zircons through connected macropores and root pathways is effective. The gneiss profiles are located downslope and the Proteroic schist series are located upslope. Within the weathering profile at Passa Quatro, the extracted zircons have similar size and morphology. Therefore, it is not possible to distinguish between autochthonous and potentially translocated zircons in the non-isostructural part of the weathering system. However, it is reasonable to neglect the possibility of translocation because the studied weathering profile is located at the top of the morphological sequence (the Dondo Mobi weathering profile is located downslope), and because no root zone has been observed (the vegetation consists of scarce grass). In addition, the total Zr content profiles do not exhibit a strong and progressive increase in the upper meters, as is the case for translocated zircon-rich zones (see Brimhall *et al.*, 1988; Colin *et al.*, 1992), our Zr content is constant throughout the saprolite in all the weathering layers toward the surface (see Table 1). Hence, at Alto das Posses Zr was used as an

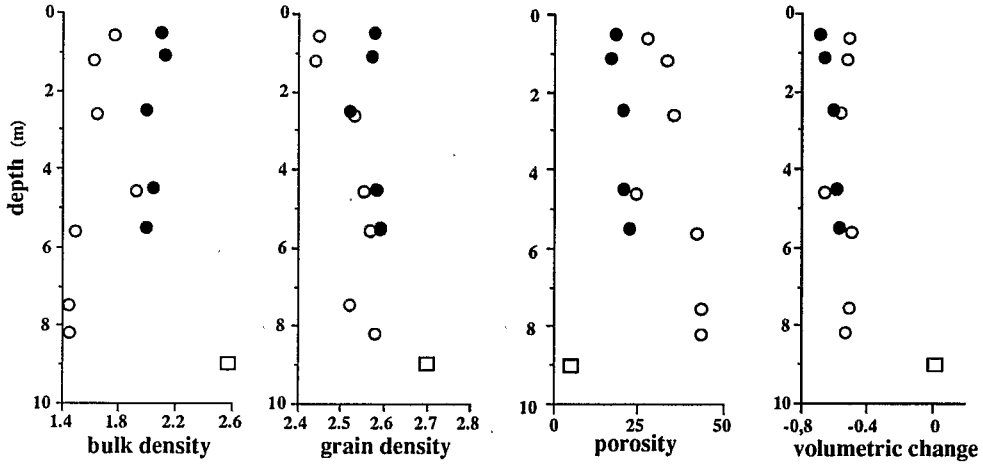


FIG. 3. Variation in bulk density (g/cm$^3$), grain density (g/cm$^3$), bulk porosity (%) and volumetric change with depth. Black circles are for matrices, white circles are for bauxitic fragments and the white square is for parent rock.

immobile index to calculate volumetric change and net gain or loss of any elements including REE.

## WEATHERING PATTERNS

The studied bauxitic weathering profile (PQA) is located at the top of a hill, whose elevation is 2190 m (Fig. 1). The average present-day precipitation is 1600 mm. The profile is 9 m deep and consists from the fresh rock to the surface of four weathering horizons, as shown in Fig. 2. Density, porosity and volumetric change are given with sample location in Table 1.

The parent rock is a nepheline syenite. Its normative composition established from chemical and petrographic analyses of five samples consists of K-feldspar (58%), nepheline (31%), ferromagnesian minerals (biotite, 1.9%, hornblende, 0.9%, ægerine-augite, 5.1%), and zircon (008%), sphene (0.74%), magnetite (1%), apatite (0.56%), and pyrochlore as accessory minerals. The bulk density (2.57), less than the measured grain density (2.70), indicates a slight porosity (≈5%) of the rock relative to the early stages of weathering.

### *Friable saprolite*

The saprolite is up to 40 cm-thick, and surrounds rounded blocks (about 1 m$^3$) of fresh syenite. The transition between fresh syenite and friable saprolite is sharp. The white saprolite is friable and the decrease of the bulk density (1.46) vs grain density (2.58) (Table 1) reflects an increase of porosity up to 43%, linked to strong dissolutional weathering. Nepheline and feldspar crystals are replaced by gibbsite, whereas pyroxene and amphibole crystals have been dissolved and partly replaced by gœthite along their cleavages and the grain surfaces. Gibbsite and gœthite form a very porous network of supergene minerals, and X-ray diffraction patterns demonstrate that they are well crystallized. In the friable saprolite, the volumetric changes reach −54%, and remain quite constant in the course of the weathering upward to the surface (Fig. 3).

### *Massive saprolite*

This saprolite is up to 2 m thick. Gibbsite is the main component of the rock (90%) while kaolinite, gœthite and anatase account for the remaining 10%. The bulk density (1.43) vs grain density (2.52) reflects a constancy of the porosity (43%). With the exception of zircon, the parent rock is totally transformed into supergene minerals, with either pseudomorphic texture after primary minerals or soil texture. This layer is cross-cut by narrow cracks (1–5 cm width), preferential paths for meteoric water partially filled with a cryptocrystalline matrix of gibbsite, gœthite and rare kaolinite.

### *Blocky saprolite*

The blocky saprolite is up to 4 m thick and cross-cut by wide cracks (>5 cm). The infilling products form a matrix around relicts of bauxitic blocks which are 40–80 cm wide. These blocks have friable cores with hard rims. Their bulk density increases from 1.49 to 1.90, the grain density is constant about 2.55, and then porosity decreases from 42 to 25%. The mineralogical components are gibbsite (90%), hematite (6%), gœthite (1%), kaolinite (2%) and anatase (1%). In the matrix the bulk density reaches the value of 2 and the porosity is 20%. It consists of gibbsite (86%), kaolinite and gœthite (6% each phase), and anatase (2%). In the lower part of this layer, dissolution voids are coated by gibbsitic and/or gœthitic cutans.

*Nodular crust*

This crust is 1–2 m thick and consists of numerous roughly indurated nodules up to 10 cm wide scattered within a gibbsite-rich matrix. Within the nodules, initial gibbsite pseudomorphs are partially replaced by a second generation of gibbsite crystals which obliterates the inherited textures. The hematite content decreases from 6 to 3%, and consequently the grain density (2.45) is lower than in the underlying layer, approaching the value of the specific gravity of gibbsite (2.40). The lower part of the layer contains numerous subhorizontal lithiophorite-rich veins. Clear structural discontinuities between the blocky saprolite and the nodular crust are defined by the reduced size of nodules and the presence of sharply limited lithiophorite-rich veins macroscopically define.

Chemical analyses of matrix and fragments from the parent rock and the derived weathering layers, as well as mass balance calculations according to Zr constant, are given for the major elements in Table 2. The main chemical changes take place during conversion of fresh rock to friable saprolite and massive saprolite. All major rock forming minerals are weathered at this stage. Alkali, alkaline-earth elements and silica are totally released from the weathering system. Aluminium, Fe and Ti are partially lost, while what remains, precipitates *in situ* to form mainly gibbsite, accessory gœthite and anatase. The significant losses of chemical elements is clearly linked to collapse (negative volumetric change). Both these chemical and physical patterns prevail within the upper weathering layers. However, the weaker losses of Al and Ti and the slight net gain in Fe differentiate the lower part of the blocky saprolite from the underlying massive saprolite. Such differentiation has to be related to cutane infillings described previously. The structural discontinuities observed at the macroscopic scale between the blocky saprolite and the nodular crust is not expressed either chemically (major elements) or mineralogically.

## REE DISTRIBUTION AND FRACTIONATION

*REE contents and chondrite-normalized patterns*

The REE analyses are listed in Tables 2 and 3, and the REE chondrite-normalized patterns are shown in Fig. 4.

In the nepheline syenite the ΣREE content is 736 ppm. The chondrite-normalized pattern exhibits a LREE enrichment relative to the HREE (ΣLREE/ΣHREE=19) and a negative Eu-anomaly (Fig. 4). The REE contents and their distribution, with $(La/Lu)_{ch}$ = 25 and Eu/Sm = 0.09 are in agreement with the results obtained by CULLERS and GRAAF (1984) for the syenite granite group.

The REE chondrite-normalized pattern of weathered rocks show a fractionation for LREE with La, Nd, Sm depletions, a positive Ce-anomaly (Ce/Ce*>2.6) (Table 3), a preserved negative Eu-anomaly and a weak fractionation of HREE. Gadolinium is systematically higher and seems most likely due to spectral interferences on Gd from $Ce^{4+}$. Consequently we have introduced a correction on the Gd values in relation to Sm and Dy contents: $Gd/Gd^* = (2Gd/Gd_{ch})/(Sm/Sm_{ch} + Dy/Dy_{ch})$ and only the Gd* values are considered in our results.

With respect to parental syenite, all REE contents decrease in the friable saprolite (440 ppm in the sample 17b), and they are more abundant in the massive saprolite (556 ppm in the sample 16b) due to high Ce contents, as indicated by the positive Ce-anomaly (Ce/Ce*=5.7). The REE increase in the transition from massive saprolite to blocky saprolite (from 842 to 1039 ppm). This increase is higher for LREE then HREE, hence the ΣLREE/ΣHREE ratios slightly increase as well as the $(La/Lu)_{ch}$ ratios (from 9 to 12), while the positive Ce-anomalies are rather constant (CE/CE* = from 4 to 6).

Compared to blocks matrices of blocky saprolite have higher REE-contents (>1200 ppm), mainly due to the significant positive Ce-anomaly. (Ce/Ce* = from 7 to 9). The ΣLREE/ΣHREE ratios, as the $(La/Lu)_{ch}$ ratios, do not vary between blocks and matrices. The highest Ce content (2171 ppm) of the 14a sample matrix, with a ratio Ce/Ce* = 18, is used to define the transition between this layer and the underlying massive saprolite.

In the nodular crust the REE ranges from 1239 to 1263 ppm for the nodules and from 1295 to 1376 ppm for the matrices. REE distributions of the nodules and matrices are similar. This feature distinguishes the discontinuity between the blocky saprolite and this surficial layer. Nevertheless, there is a smooth variation in the REE.

REE of some pit P-132 (Fig. 1) samples have also been analysed. The weathering profile observed in this pit consists of a nodular bauxitic layer in its upper part, similar to that observed upslope, and bauxitic blocks embedded in a kaolinitic matrix in its lower part. The REE patterns, normalized to the chondrites are shown Fig. 7. The REE contents of bauxitic blocks range from 345 to 1003 ppm, and the REE contents of the kaolinitic matrix vary from 702 to 1239 ppm. The fractionation between LREE and HREE in this kaolinitic profile is similar to those calculated for the samples collected from the bauxitic profile PQA, including a positive Ce anomaly of 3 in the weathered blocks and 6–15 in the kaolinite.

*REE mass balance normalized to parent rock*

Mass balances calculated with respect to the parent rock are reported in Table 2 and shown in Fig. 5. It is clear that all the weathered rocks are strongly depleted in REE. The only gain in REE was in the

Table 2. Major elements (wt%) are rare earth elements (ppm) of the samples from PQA profile. The grains ($\tau > 0$) and the losses ($\tau < 0$) based on the Zr constant in relation to the syenite

| | Nodular crust | | | | Blocky saprolite | | | | | | Massive saprolite | Friable saprolite | Syenite |
|---|---|---|---|---|---|---|---|---|---|---|---|---|---|
| Sample | 2b | 2a | 5b | 5a | 8b | 8a | 13b | 13a | 14b | 14a | 16b | 17b | 17c |
| $SiO_2$ | 1.78 | 1.76 | 1.67 | 3.02 | 1.96 | 4.76 | 1.12 | 1.78 | 0.51 | 0.53 | 0.52 | 0.64 | 54.20 |
| $Al_2O_3$ | 59.86 | 59.00 | 57.50 | 56.10 | 59.13 | 55.65 | 60.00 | 57.00 | 59.00 | 58.20 | 59.00 | 58.00 | 21.00 |
| $Fe_2O_3$ | 4.80 | 5.90 | 5.60 | 8.22 | 5.59 | 6.69 | 5.67 | 7.51 | 8.14 | 7.84 | 7.60 | 5.85 | 2.06 |
| MgO | 0 | 0 | 0 | 0 | 0 | 0 | 0 | 0 | 0 | 0 | 0 | 0 | 0 |
| CaO | 0.03 | 0.05 | 0.35 | 0.14 | 0.06 | 0.01 | 0.37 | 0.21 | 0.17 | 0.09 | 0.04 | 0.01 | 1.61 |
| $Na_2O$ | 0 | 0 | 0 | 0 | 0 | 0 | 0 | 0 | 0 | 0 | 0 | 0 | 7.30 |
| $K_2O$ | 0.18 | 0.20 | 0.14 | 0.36 | 0.39 | 0.73 | 0.16 | 0.31 | 0 | 0 | 0.22 | 0.05 | 7.90 |
| $TiO_2$ | 0.83 | 1.18 | 1.07 | 1.49 | 1.21 | 1.29 | 0.97 | 1.66 | 1.30 | 1.87 | 2.09 | 1.37 | 0.62 |
| MnO | 0.19 | 0.24 | 0.20 | 0.30 | 0.10 | 0.20 | 0.13 | 0.22 | 0.22 | 0.20 | 0.22 | 2.79 | 0.13 |
| $H_2O$ | 31.50 | 31.42 | 31.40 | 29.25 | 31.20 | 29.12 | 31.65 | 30.61 | 31.05 | 30.57 | 31.02 | 30.88 | 1.87 |
| Total | 99.17 | 99.75 | 97.93 | 98.88 | 99.64 | 98.45 | 100.07 | 99.30 | 100.39 | 99.30 | 100.71 | 99.59 | 97.03 |
| La | 125.57 | 113.32 | 105.68 | 88.28 | 96.46 | 75.29 | 121.27 | 104.41 | 78.63 | 60.22 | 52.96 | 68.40 | 176.23 |
| Ce | 1033.32 | 1152.84 | 1051.00 | 1127.68 | 870.9 | 1146.59 | 843.12 | 1114 | 694.32 | 2048.21 | 461.90 | 310.92 | 368.30 |
| Nd | 50.71 | 65.60 | 63.58 | 46.25 | 43.83 | 33.62 | 55.03 | 43.28 | 41.06 | 35.72 | 23.96 | 37.08 | 134.03 |
| Sm | 6.90 | 9.61 | 9.21 | 6.65 | 6.11 | 4.90 | 7.82 | 6.07 | 5.96 | 5.14 | 3.45 | 5.36 | 18.51 |
| Eu | 0.94 | 1.23 | 1.19 | 1.02 | 0.87 | 0.77 | 0.95 | 0.91 | 0.78 | 1.02 | 0.58 | 0.64 | 1.77 |
| Gd | 6.93 | 9.93 | 9.71 | 7.20 | 5.22 | 5.22 | 6.31 | 6.31 | 6.04 | 6.04 | 3.73 | 5.25 | 16.48 |
| Dy | 5.82 | 8.78 | 8.90 | 6.89 | 5.53 | 4.87 | 6.33 | 5.65 | 5.89 | 6.5 | 3.57 | 4.18 | 10.35 |
| Er | 3.60 | 5.97 | 5.79 | 4.69 | 3.83 | 3.26 | 4.52 | 3.79 | 3.98 | 3.73 | 2.66 | 3.55 | 5.40 |
| Yb | 4.41 | 8.01 | 7.13 | 5.71 | 4.75 | 3.85 | 5.42 | 4.73 | 4.50 | 4.22 | 3.54 | 4.23 | 4.27 |
| Lu | 0.84 | 1.34 | 1.19 | 1.02 | 0.86 | 0.66 | 0.99 | 0.83 | 0.79 | 0.74 | 0.60 | 0.77 | 0.72 |
| ΣREE | 1239.04 | 1376.63 | 1263.38 | 1295.39 | 1038.36 | 1279.03 | 1051.76 | 1289.98 | 841.95 | 2171.54 | 556.95 | 440.38 | 736.06 |
| $\tau_{Si}$ | −0.99 | −0.99 | −0.99 | −0.98 | −0.99 | −0.97 | −0.99 | −0.99 | −1.0 | −1.00 | −1.00 | −1.00 | 0 |
| $\tau_{Al}$ | −0.06 | −0.31 | −0.18 | −0.27 | −0.21 | −0.19 | −0.29 | −0.11 | −0.18 | −0.07 | −0.24 | −0.28 | 0 |
| $\tau_{Fe}$ | −0.23 | −0.30 | −0.19 | 0.09 | −0.24 | −0.01 | −0.32 | 0.19 | 0.16 | 0.27 | 0.00 | −0.26 | 0 |
| $\tau_{Ti}$ | −0.56 | −0.54 | −0.48 | −0.34 | −0.45 | −0.36 | −0.61 | −0.12 | −0.38 | 0.04 | −0.09 | −0.42 | 0 |
| $\tau_{La}$ | −0.77 | −0.84 | −0.82 | −0.86 | −0.85 | −0.87 | −0.83 | −0.81 | −0.87 | −0.89 | −0.92 | −0.90 | 0 |
| $\tau_{Ce}$ | −0.08 | −0.24 | −0.15 | −0.16 | −0.34 | −0.05 | −0.44 | −0.02 | −0.45 | 0.85 | −0.66 | −0.78 | 0 |
| $\tau_{Nd}$ | −0.88 | −0.88 | −0.86 | −0.91 | −0.91 | −0.92 | −0.90 | −0.89 | −0.91 | −0.91 | −0.95 | −0.93 | 0 |
| $\tau_{Sm}$ | −0.88 | −0.87 | −0.85 | −0.90 | −0.91 | −0.92 | −0.90 | −0.89 | −0.91 | −0.91 | −0.95 | −0.92 | 0 |
| $\tau_{Eu}$ | −0.83 | −0.83 | −0.80 | −0.84 | −0.86 | −0.87 | −0.87 | −0.83 | −0.87 | −0.81 | −0.91 | −0.91 | 0 |
| $\tau_{Gd}$ | −0.86 | −0.85 | −0.82 | −0.88 | −0.89 | −0.90 | −0.88 | −0.88 | −0.89 | −0.88 | −0.94 | −0.92 | 0 |
| $\tau_{Dy}$ | −0.82 | −0.79 | −0.74 | −0.82 | −0.85 | −0.86 | −0.85 | −0.82 | −0.83 | −0.79 | −0.91 | −0.90 | 0 |
| $\tau_{Er}$ | −0.78 | −0.73 | −0.68 | −0.76 | −0.80 | −0.82 | −0.79 | −0.77 | −0.78 | −0.77 | −0.87 | −0.83 | 0 |
| $\tau_{Yb}$ | −0.66 | −0.54 | −0.50 | −0,64 | −0.69 | −0.72 | −0.69 | −0.64 | −0.69 | −0.67 | −0.78 | −0.74 | 0 |
| $\tau_{Lu}$ | −0.62 | −0.55 | −0.51 | −0.61 | −0.67 | −0.72 | −0.66 | −0.62 | −0.68 | −0.66 | −0.78 | −0.72 | 0 |
| $\tau_{Zr}$ | 0 | 0 | 0 | 0 | 0 | 0 | 0 | 0 | 0 | 0 | 0 | 0 | 0 |

Table 3. Total REE, LREE and HREE contents throughout the bauxitic profile PQA; normalized chondrite LREE/HREE ratios except Ce, Ce/HREE ratios, La/Lu ratios; Ce anomaly = Ce/Ce* = $(3Ce/Ce_{ch}/(2La/La_{ch} + Nd/Nd_{ch})$; for samples numbers, a is related to matrices, b to bauxitic fragments and c to nepheline syenite

| Sample | ΣREE | ΣLREE | ΣHREE | $(\Sigma LREE/\Sigma HREE)_{ch}$ except Ce | $(Ce/\Sigma HREE)_{ch}$ | $(La/Lu)_{ch}$ | Ce/Ce* |
|---|---|---|---|---|---|---|---|
| 2b | 1239.04 | 1217.44 | 21.60 | 4.93 | 11.77 | 15 | 5.3 |
| 2a | 1376.63 | 1342.60 | 34.03 | 3.11 | 8.23 | 9 | 5.6 |
| 5b | 1263.38 | 1230.66 | 32.72 | 3.12 | 7.97 | 9 | 4.9 |
| 5a | 1295.39 | 1269.88 | 25.51 | 3.14 | 10.74 | 9 | 7.5 |
| 8b | 1039.43 | 1018.17 | 21.26 | 3.92 | 9.92 | 12 | 5.8 |
| 8a | 1279.03 | 1261.17 | 17.86 | 3.73 | 15.87 | 12 | 9.7 |
| 13b | 1051.76 | 1028.19 | 25.01 | 4.20 | 8.20 | 13 | 4.1 |
| 13a | 1289.98 | 1268.67 | 21.31 | 4.18 | 12.77 | 13 | 6.7 |
| 14b | 841.95 | 820.75 | 21.50 | 3.37 | 8.00 | 10 | 4.9 |
| 14a | 2171.54 | 2150.31 | 21.23 | 2.82 | 24.36 | 9 | 18.5 |
| 16b | 556.95 | 542.85 | 14.10 | 3.21 | 7.78 | 9 | 5.7 |
| 17b | 440.38 | 422.40 | 17.98 | 3.39 | 4.10 | 9 | 2.6 |
| 17c | 736.06 | 698.84 | 37.22 | 5.55 | 2.78 | 25 | 1 |

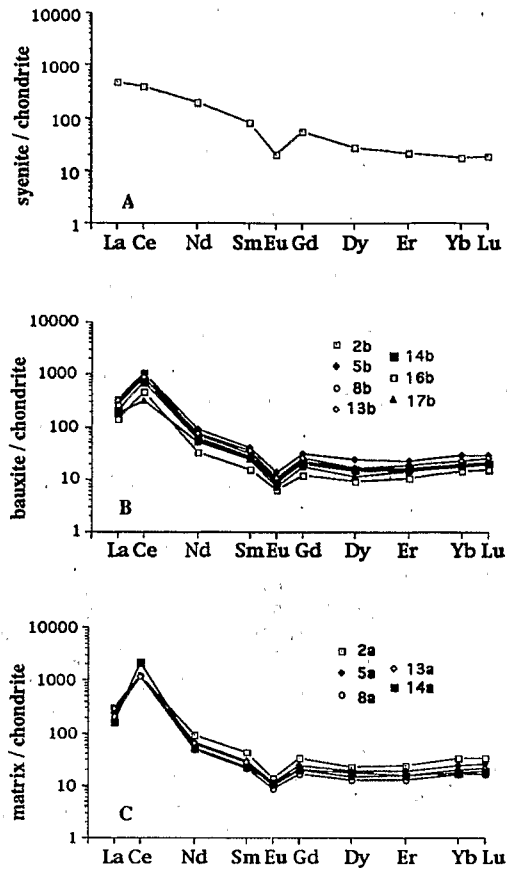


FIG. 4. REE chondrite normalized patterns. (A) Nepheline syenite, (B) bauxitic fragments and (C) matrices.

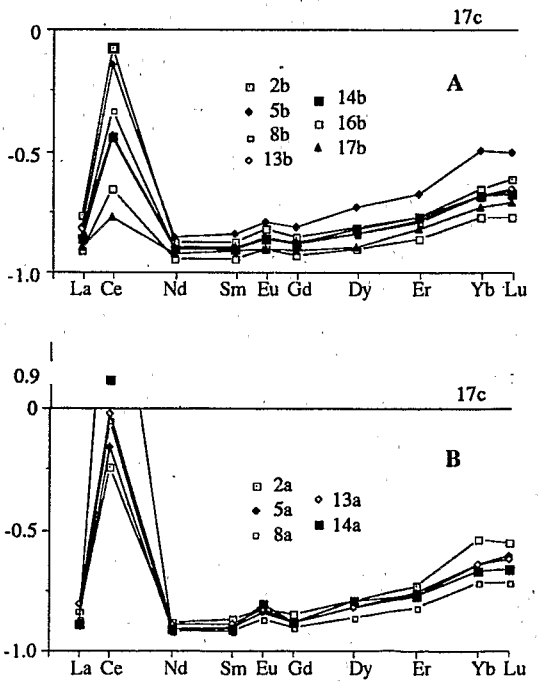


FIG. 5. REE net mass transport function patterns ($\tau$) within the whole profile. For example number, (A) is related to bauxitic fragments and (B) is related to matrices.

matrix 14a, which shows a net Ce mass gain, according to the high ratio Ce/Ce*. However, detailed examinations of REE mass balance calculations by layers gives information on the step by step gains and losses of REE during weathering. This can be done for each weathering layer by calculating the total mass of transferred elements ($m_{REE,w}$) during the conversion of a given layer to another given layer, for example by considering that each layer($n$) generates by increasing weathering from the underlying layer ($n-1$) as indicated by Eqn (4):

$$m_{REE,w} = (\tau_{REE,w_n} - \tau_{REE,w_{n-1}})\, C_{REE,p}\, \rho_p \quad (4)$$

with the following dimensional equation:

$$[g]\,[m]^{-3} = [g]\,[t]^{-1}\,[t]\,[m]^{-3}.$$

The results are presented graphically depicted in Fig. 6.

Weathering of syenite to form the friable saprolite results in significant losses in all REE (Fig. 6A). Concerning the LREE, the mass losses of Ce account for 740 g/m$^3$ (−78%), the mass losses of La and Nd account each for about 400 g/m$^3$, whereas for Sm the mass loss is about 30 g/m$^3$; the mass loss of Eu accounts for no more than 4 g/m$^3$, in relation to the primary negative anomaly of Eu in the fresh syenite. Concerning the HREE, the mass losses range from 30 g/m$^3$ for Gd to 10 g/m$^3$ for Yb. The mass loss of Lu is very weak. The difference between the depletive transport function for LREE (−91%), except Ce, and for HREE (−82%) with respect to the parent rock indicates a slight fractionation of REE during weathering.

The losses of REE increase from the friable saprolite to the massive saprolite (Fig. 6B), while the alkali and alkaline-earths are totally leached during the first stages of weathering (Table 2). It appears that the release of REE occurs later compared to the loss of the major elements in the course of weathering. Nevertheless the transport function for HREE (−1 to −6%) is greater than those calculated for LREE (−2 to −3%). Ce is enriched by 112 g/m$^3$, while the Eu mass loss is very weak and not significant.

From the massive saprolite to the blocky saprolite, the calculations of the mass indicate weak gains, more important for LREE than HREE, as shown in the Fig. 6C. In the bauxitic blocks, the La and Nd gains are, respectively, 40 and 20 g/m$^3$, Ce is strongly enriched (700 g/m$^3$), and the Eu gain is not significative. These gains are always higher in the matrix than in the blocks, reaching maximum values for sample 14a which correlates to the high Ce gain (+85% compared to the parent rock).

During conversion of the blocky saprolite into the nodular crust (Fig. 6D), we note a REE gain of about 10 g/m$^3$ for the LREE and 1 g/m$^3$ for the HREE. In contrast, there is a Ce loss of 79 g/m$^3$.

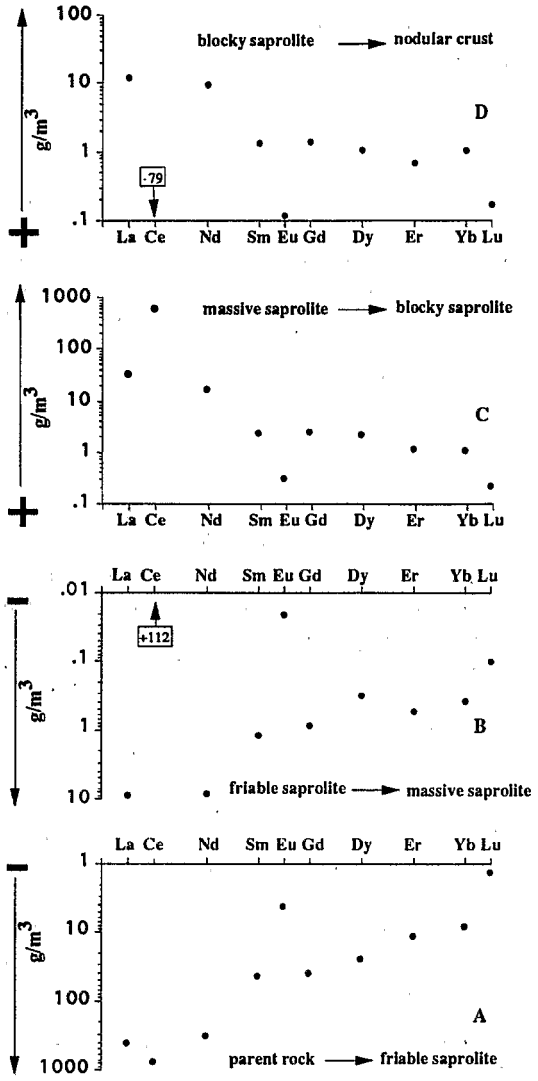


FIG. 6. REE volumetric mass gains and losses ($g/m^3$) patterns calculated from layer to layer toward the surface; (A) from parent rock to friable saprolite; (B) from friable saprolite to massive saprolite; (C) from massive saprolite to blocky saprolite; and (D) from blocky saprolite to nodular crust.

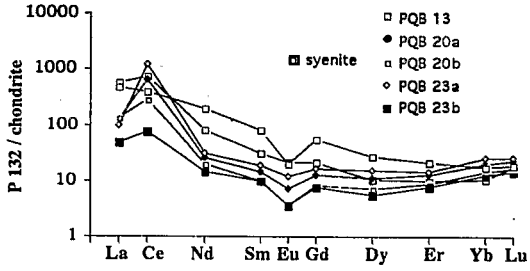


FIG. 7. REE chondrite normalized patterns for the kaolinitic sample of the P.132 profile located downslope.

## DISCUSSION

Occurrences of bauxite as a result of the weathering of syenite are reported in Guinea (BONIFAS, 1959), Arkansas (GORDON *et al.*, 1958) and Cameroon (BILONG, 1988). These bauxite deposits are clearly considered as formed by "direct bauxitization" processes, resulting from initial development of gibbsite from the weathering of nepheline and feldspar, as well as gœthite after ferromagnesian primary minerals. In most cases, supergene minerals were reported as pseudomorphs after primary minerals and then the replacement was considered isovolumetric as defined by MILLOT and BONIFAS (1955). We demonstrate that at Passa Quatro bauxitization processes have generated volumetric changes approximately −50% ($\varepsilon_{Zr}$), compared to the fresh syenite, since the earliest stage of weathering. By taking into account such strain, mass balance calculations demonstrate that certain elements are strongly released out of the weathering system. Aluminium, Fe and Ti are the less mobile elements. By applying isovolumetric calculations on bauxites from Iles de Los, BONIFAS (1959) found that Al was imported from external sources with more than 40% added with respect to the parent rock. In a similar weathering profile, we conclude that there has been a net Al mass loss of 20% with respect to the parent rock. This Al loss from soils is in agreement with the results obtained in a study of African bauxite deposits (BOULANGÉ, 1984); spring and ground waters issued from the bauxitic plateau contain from 0.20 to 0.60 mg/l of $Al_2O_3$ and that such amounts of Al are released from soils at a rate of 20 $mg/cm^3$ 1000 a.

An important point to be noticed is the thickness of the friable saprolite, which is a less than 50 cm thick cortex. Within this weathered layer, the volumetric change, still reaches −50% and net mass losses of most of the elements are drastic during these first stages of weathering compared to the remaining upper weathering layers. Upward within the overlying layers, volumetric change ranges from −50 to −70% typically with higher values for matrices than for indurated blocks. The conversion from massive saprolite to blocky saprolite produces a slight enrichment in Fe ($\tau_{Fe}$ ranging from +16 to +27%). This downward movement of iron manifests itself as gœthite-rich cutans coating dissolution voids at the top of the massive saprolite (BOULANGÉ *et al.*, 1975; BOCQUIER *et al.*, 1985). Such weathering, taking place under prevailing strong dissolutional conditions, causes a fractionation and leaching of the REE elements.

In a study of the REE distributions among minerals in a granodiorite (GROMET and SILVER, 1983) note the high REE concentrations in primary minerals such as sphene and apatite, and the low REE concentrations in the feldspars and biotite, with high HREE concentration in zircon. The minerals being weathered are chronologically: nepheline, K-feldspar, pyr-

oxene, amphibole, biotite, apatite and sphene. Their dissolution leads to a cumulative strong removal of all the REE, weaker for Ce and HREE.

The slightly late REE release compared to the release of major elements, from the friable to the massive saprolite, is linked to the differential weathering of the REE-bearing minerals, apatite and sphene. Apatite weathers first simultaneously to nepheline and feldspars, while sphene weathers later within the massive saprolite. As a consequence, the net mass losses of all REE, but Ce, increase from the friable saprolite to the massive saprolite (Fig. 6B). Cerium can partly reprecipitate as $Ce^{3+}$ in secondary florencite $(La,CE)Al_3(PO_4)_2(OH)_6$, a phase which has been observed under the SEM. We have also noted that under high oxidation conditions, $Ce^{4+}$ could form, mineralogically expressed as cerianite (BRAUN *et al.*, 1990). However this mineral has not been found within the profile.

The Ce-anomaly is attributed to the weathering of apatites and sphene, and also to the stability of zircons. Zircons, whose size is below 50 $\mu$m, are frequently associated with sphenes in the parent materials. Such zircons have their original euhedral habit, and do not exhibit any weathering features. Typically high HREE contents and positive Ce anomalies are found in zircons (MURALI *et al.*, 1983; HINTON and UPTON, 1991). HINTON and UPTON (1991) have established that a syenite has an apparent Ce zircon/melt partition coefficient of 1.1. These authors have shown that the Ce-positive anomaly in zircon is due to "the significant ability of $Ce^{4+}$ to fit in the zircon structure" because of the similar oxidation state of Zr and Ce, and because of the comparable ionic radii. At Passa Quatro, the values of the ratio $(Ce/\Sigma HREE)_{ch}$ (Table 3) range from 3 for the fresh syenite to approximately 8 for the bauxitic fragments (16b to 8b). Within the bauxitic fragments, the constancy of this ratio demonstrates clearly a relationship between the Ce-positive anomaly and the presence of weathering-resistant zircons. Conversely, the strong variation (10 to 24) of this ratio within the matrices (14a to 8a) indicate that Ce is (probably chemically) mobile within such preferential circulation paths.

The mass balance calculations done with Zr as an immobile index demonstrate that all the REE, but particularly the LREE, are strongly leached during weathering while Ce and HREE present in zircons remain as residual element.

However, to be accurate such calculations have to be carried out by considering the parental material chemically homogeneous. To discuss the degree of homogeneity, it is necessary to compare the distribution of elements such as Al, Fe, and Ti.

If the Ti content of syenite (17c) was 0.32% rather then 0.37%, applying the same method of calculation for the volumetric change considering Al, Fe and Ti successively constant, the parameters $\varepsilon_{i,w}$ [Eqn (2)] would be very similar (respectively $-0.36$, $-0.38$, $-0.31$). These results suggest that relative to the most abundant of these (Al and Fe), there is slight inhomogeneity in Ti (approximately 15%). This is reasonable considering that Ti is only a quarter as abundant as the total Al residing primarily in feldspars and feldspathoids in the parent syenite and Fe residing primarily in biotite. Titanium resides in biotite and accessory phases (sphene). These minerals react with soil waters at different rates, consequently a reasonable explanation for the similar ratios is that, during formation of the friable saprolite, they were all effectively conserved. Thus, considering Ti constant, with $\varepsilon_{i,w} = -0.31$, the Zr gain ($\tau_{Zr}=+0.50$) in friable saprolite (17b) is very high compared to Al and Fe gains ($\tau_{Al}=+0.08$ and $\tau_{Fe}=+0.11$) and the most likely explanation is that Zr could be inhomogeneously distributed in the parent rock.

Using Ti as a constant, the REE losses can be calculated by the same method [Eqn (3)]. Percentage REE losses ($\tau$) present a slight variation compared to the values obtained with Zr (Table 2). The losses of LREE, except Ce, are about 6% lower, and the losses of HREE and Ce are about 15–20%. This high difference obtained for Ce and HREE in these calculations confirms the relation between these elements and zircon. In the massive saprolite, the volumetric change calculated with Zr as the immobile index is similar to the volumetric change calculated with Ti and accordingly the net mass REE losses are equal.

Consequently, the mass balance calculations done with either Zr (or Ti) as immobile index demonstrate that all the REE are leached during the formation of the friable saprolite but preferentially the light REE. A most interesting aspect is that Ce and HREE (Dy, Er and Lu) are less leached than other REE's, due to the fact that a part of these elements are included within the zircons.

Considering that the REE contents are low, we have to be cautious in interpreting the results related to both the blocky saprolite and the nodular saprolite and in this way only a tendency can be significantly deduced. Compared to the base of the weathering profile, REE losses are lower within the blocky saprolite as well as within the surficial nodular crust (Table 2). This revealed a REE gain with respect to the underlying layers (Fig. 6). In addition, Al and Fe are enriched, correlating to the presence of gœthitic cutanes. This relationship points out the possible role of gœthite as providing preferential adsorption sites for the REE (FLEET, 1984). In the surficial nodular crust, only Ce is strongly leached out of the surficial layer ($-79$ g/m$^3$ with respect to the blocky saprolite). Except for Ce, REE distribution does not emphasize the macroscopic discontinuity expressed at the scale of the weathering profile by lithiophorite-rich veins between the blocky saprolite and the nodular crust.

Dissolution processes during bauxitization provoke strong REE leaching. This intense REE leaching has also to be related to the lack of exchange sites

or to the weak adsorption capacity of gibbsite crystals. In similar acidic conditions, adsorption on the surfaces of smectitic or kaolinitic minerals have been reported (Balashov *et al.*, 1964; Roaldset, 1979; Decarreau *et al.*, 1979) and the authors suggested either a weak REE removal (Aagard, 1974; Nesbitt, 1979; Decarreau *et al.*, 1979; Bonnot-Courtois, 1981), or simple REE immobility (Piper, 1974). In the Passa Quatro bauxitic profile, the weathering intensity induced the development of an important porosity and the almost exhaustive formation of gibbsite reducing the possibility for REE to stabilize *in situ*.

In spite of the strong losses of REE due to weathering of the nepheline syenite, REE distribution and behaviour points out a geochemical discontinuity between the lower part of the profile (friable and massive saprolite) and the blocky saprolite. The lower part defines a REE depletive compartment which characterizes the *in situ* chemical lowering while the blocky saprolite differentiates a REE enriched compartment (with respect to the lower part) which identify external input. Nevertheless, the studied weathering system is located at the hill top and therefore we interpret the external input as a result of downward chemical transfer having taken place during reduction of the previous regolith. Sigolo (1988) established that two periods of bauxitization occurred in this area: the first is estimated as late Cretaceous–Eocene age, and the second period Miocene to present time. This demonstrates that, in this region, the structural discontinuity between the nodular crust and the blocky saprolite could be reflecting these two bauxitic episodes. We propose that imported REE in the upper part of the profile, with respect to the lower part, reflect the previous bauxitic episode.

We have demonstrated that the bauxitization processes involved in the weathering of the Passa Quatro syenite caused significant losses in REE. In addition, the chondrite normalized pattern of REE of downslope kaolinites (see pit 132, Figs 1 and 7) shows a negative anomaly of all the REE but Ce, Yb and Lu, linked to zircon. However, the lack of significant REE gain demonstrates that these kaolinites are not efficient traps of REE.

Consequently, on the regional scale, sediments will probably be enriched in REE. Simultaneously to the Eocene–Oligocene uplift of the "Serra do Mar" (Passa Quatro massif is a part of the Serra do Mar), the Paraiba graben opened inducing the development of regional scale basins, such as for example the Curitiba basin. Fortin (1989) established that the Curitiba sediments are REE enriched with respect to NASC shales. The author stressed that the absolute mass gains in Nd, Sm, Eu, Gd and Er are higher than the gains in La, Ce, Yb and Lu and that such patterns are in agreement with the REE-fractionation having taken place during weathering. In addition, by studying the parental rocks of these sediments, Fortin (1989) showed that the $^{87}Sr/^{86}Sr$ and $^{143}Nd/^{144}Nd$ ratios reflect the chemical signature of the Tunas nepheline syenites of the southern part of the Serra do Mar.

## CONCLUSIONS

The results obtained in this study allow us to draw five essential conclusions.

(1) During the conversion of the Passa Quatro nepheline syenite into lateritic bauxite, the weathering of apatites and sphenes induces the release of most of the primary REE initially concentrated in syenite.

(2) Bauxitization processes provoke a net mass loss of all the REE, with a fractionation between LREE and HREE, expressed by a lower rate of loss of the HREE. This intense REE leaching has also to be related to the lack of exchange sites according to the weak adsorption capacity of gibbsite.

(3) The positive correlation between Ce and the HREE is consistent with the occurrence of a part of these elements within zircons, which are resistant to weathering and accumulate relative to major components by collapse of the bauxitic regolith.

(4) Cerium exhibits a very strong positive anomaly due to: (i) the $Ce^{3+}$ precipitated in authigenic florencite; (ii) the primary $Ce^{4+}$ of residual zircons; and (iii) probably the $Ce^{4+}$ formed from the oxidation of $Ce^{3+}$ and included within cerianite.

(5) The downslope kaolinitic-rich weathering systems are not efficient traps for the REE leached from the upslope gibbsitic-rich systems. As a consequence, sedimentary processes taking place in the continuation of weathering processes might have led to the enrichment in REE of the Paraiba basins.

*Acknowledgements*—Financial support for this study was provided by ORSTOM and USP (Universidade de São Paulo, Brazil) and we thank Prof. A. Melfi for having initiated this study, and J. Sigolo for participation in field studies. This paper has benefited from a pre-review by A. Michard and from very constructive reviews by R. W. Hinton, B. Hitchon and one anonymous reviewer. Collaboration and dialogues with J. P. Muller and C. Parron are much appreciated. English language has been greatly improved by C. Elliott. We also thank J. J. Motte for artwork.

*Editorial handling*: Yves Tardy.

## REFERENCES

Aagard P. (1974) Rare earth elements adsorption on clay minerals. *Bull. Groupe Fr. Argiles.* **26**, 193–199.

Alderton D. H. M., Pearce J. A. and Potts P. J. (1980) Rare earth elements mobility during granite alteration: evidence from southwest England. *Earth Planet. Sci. Lett.* **49**, 149–165.

Balashov Y. A., Ronov A. B., Migdisov A. A. and

TURANSKAYA N. V. (1964) The effects of climate and facies environment on the fractionation of rare earths during sedimentation. *Geochem. Int.* **10**, 951–969.

BILONG P. (1988) Genèse et développement des sols ferrallitiques sur syénite alcaline potassique en milieu forestier du centre-sud Cameroun. Comparaison avec les sols ferrallitiques développés sur roches basiques. Ph.D. dissertation, University of Yaoundé Cameroun.

BOCQUIER G., MULLER J. P. and BOULANGE B (1985) Les latérites. Connaissances et perspectives. In *Livre Jubilaire Cinquantenaire Ass. Française pour l'Etude du Sol*, pp. 123–138.

BONIFAS M. (1959) Contribution à l'étude géochimique de l'altération latéritique. *Mém. Serv. Carte Géol. Alsace. Lorraine* **17**.

BONNOT-COURTOIS C. (1981) Géochimie des terres rares dans les principaux milieux de formation et de sédimentation des argiles Thèse Dr. Sci., Université de Paris Sud, Orsay.

BOULANGÉ B. (1984) Les formations bauxitiques latéritiques de Côte d'Ivoire. Trav. Doc., ORSTOM, Paris, 175.

BOULANGÉ B., PAQUET H. and BOCQUIER G. (1975) Le rôle de l'argile dans la migration et l'accumulation de l'alumine de certaines bauxites tropicales. *C.r. Acad. Sci., Paris* **280D**, 2183–2186.

BRAUN J. J., PAGEL M., MULLER J. P., BILONG P., MICHARD A. and GUILLET B. (1990) Cerium anomalies in lateritic profiles. *Geochim. cosmochim. Acta* **54**, 781–795.

BRIMHALL G. H. AND DIETRICH W. E. (1987) Constitutive mass balance relations between chemical composition, volume, density, porosity, and strain in metasomatic hydrochemical systems: results on weathering and pedogenesis. *Geochim. cosmochim. Acta* **51**, 567–587.

BRIMHALL G. H., LEWIS C. J., AGUE J. J., DIETRICH W. E., HAMPEL J., TEAGUE T. and RIX P. (1988) metal enrichment in bauxites by deposition of chemically mature aeolian dust. *Nature* **333**, 819–824.

COLIN F., BRIMHALL G. H., NAHON D., BARONNET A. and KATHY D. (1992) Equatorial rainforest lateritic mantles: a geomembrane filter. *Geology* **20**, 523–526.

CULLERS R. F. and GRAAF J. L. (1984) Rare earth elements in igneous rocks of the continental crust: predominantly basic and ultrabasic rocks. In *Rare Earth Elements Geochemistry* (ed. P. HENDERSON), pp. 237–275. Elsevier, Amsterdam.

DECARREAU A., COURTOIS C. and STEINBERG M. (1979) Comportement des éléments de la première série de transition et des lanthanides dans les altérations naturelles et expérimentales. Publ. ERA No, 765 du CNRS, pp. 29–34.

DUDDY I. R. (1980) Redistribution and fractionation of rare earth and other elements in a weathering profile. *Chem. Geol.* **30**, 363–381.

FLEET A. J. (1984) Aqueous and sedimentary geochemistry of the rare earth elements. In *Rare Earth Elements Geochemistry* (ed. P. HENDERSON), pp. 343–373. Elsevier, Amsterdam.

FORTIN P. (1989) Mobilisation, fractionnement et accumulation des terres rares lors de l'altération latéritique de sédiments argilo-sableux du bassin de Curitiba (Brésil). *Mém. Sci. de la Terre* **10**.

GORDON M., TRACEY J. L. and ELLIS M. W. (1958) Geology of the Arkansas bauxite region. U.S. Geol. Survey Prof. Paper 299.

GOVINDARAJU K. and MEVELLE G. (1987) Fully automated dissolution and separation methods for inductively coupled plasma atomic emission spectrometry rock analysis. Application to the determination of rare earth elements. Plenary lecture. *J. Analyt. Atom. Spectr.* **2**, 615–621.

GROMET P. L. and SILVER L. T. (1983) Rare earth element distributions among minerals in a granodiorite and their petrogenic implications. *Geochim. cosmochim. Acta* **47**, 925–939.

HINTON R. W. and UPTON B. G. J. (1991) The chemistry of zircon: Variations within and between large crystals from syenite and alkali basalt xenoliths. *Geochim. cosmochim. Acta* **55**, 3287–3302.

LAUFER F., YARIV S. and STEINBERG M. (1984) The adsorption of quadrivalent cerium by kaolinite. *Clay Miner.* **19**, 137–149.

MAKSIMOVIC Z. and ROALDSET E. (1976) Lanthanide elements in some Mediterranean karstic bauxite deposits. *Travaux ICSOBA* **13**, 199–220.

MAKSIMOVIC Z. and PANTÓ G. (1985) Neodymian goyazite in the bauxite deposit of Vlasenica, Yugoslavia. *TMPM Tschermaks Miner. Petrol. Mitt.* **34**, 159–165.

MCLENNAN S. M. (1989) Rare earth elements in sedimentary rocks: influence of provenance and sedimentary processes. In *Geochemistry and Mineralogy of Rare Earth Elements* (eds B. R. LIPIN and G. A. MCKAY). *Miner. Soc. Am. Rev. Miner.* **21**, 169–196.

MIDDELBURG J. J., VAN DER WEIDJEN C. H. and WOITTIEZ J. R. W. (188) Chemical processes affecting the mobility of major, minor and trace elements during weathering of granitic rocks. *Chem. Geol.* **68**, 253–273.

MILLOT G. and BONIFAS M. (1955) Transformations isovolumétriques dans les phénomènes de latéritisation et de bauxitisation. *Bull. Serv. Carte Géol. Alsace. Lorraine* **8**, 3–10.

MURALI A. V., PARTHASARATY R., MAHADEVAN T. M. and SANKAR DAS M. (1983) Trace elements characteristics, REE patterns and partition coefficients of zircons from different geological environments. A case study on Indian zircons. *Geochim. cosmochim. Acta* **47**, 2047–2052.

NESBITT H. W. (1979) Mobility and fractionation of rare earth elements during weathering of a granodiorite. *Nature* **279**, 206–210.

PIPER D. Z. (1974) Rare earth elements in the sedimentary cycle: a summary. *Chem. Geol.* **14**, 285–304.

ROALDSET E. (1973) Rare earth elements in Quaternary clays of the Numedal area, southern Norway. *Lithos* **6**, 349–372.

ROALDSET E. (1979) Rare earth elements in different size fractions of a marine quick clay from Ullensaker, and a till from Upper Numedal, Norway. *Clay Miner.* **14**, 229–240.

RONOV A. B., BALASHOV Y. A. and MIGDISOV A. A. (1967) Geochemistry of the rare earths in the sedimentary cycle. *Geochem. Int.* **4**, 1–17.

SIGOLO J. B. (1988) As formações bauxíticas lateríticas do maciço alcalino de Passa Quatro, MG. Th. Doct., USP, São Paulo, Brazil.

SIGOLO J. B. and BOULANGÉ B. (1987) Caracterização das facies de alteração de uma topossequência no maciço alcalino de Passa Quatro (MG). *Rev. Brasil. Geocien.* **17**, 269–275.

STEINBERG M. and COURTOIS C. (1976) Le comportement des terres rares au cours de l'altération et ses conséquences. *Bull. Soc. Géol. Fr.* **18**, 13–20.

ULBRICH H. H. G. J. and GOMES C. B. (1981) Alkaline rocks from continental Brasil. *Earth Sci. Rev.* **17**, 135–154.